Check for updates

ADVANCED HEALTHCARE MATERIALS
www.advhealthmat.de

Amphiphilic Single-Chain Polymer Nanoparticles as Imaging and Far-Red Photokilling Agents for Photodynamic Therapy in Zebrafish Embryo Xenografts

Davide Arena, Christophe Nguyen, Lamiaa M. A. Ali, Ester Verde-Sesto, Amaia Iturrospe, Arantxa Arbe, Umit İşci, Zeynel Şahin, Fabienne Dumoulin, Magali Gary-Bobo,* and José A. Pomposo**

This work introduces rationally designed, improved amphiphilic single-chain polymer nanoparticles (SCNPs) for imaging and photodynamic therapy (PDT) in zebrafish embryo xenografts. SCNPs are ultrasmall polymeric nanoparticles with sizes similar to proteins, making them ideal for biomedical applications. Amphiphilic SCNPs result from the self-assembly in water of isolated synthetic polymeric chains through intrachain hydrophobic interactions, mimicking natural biomacromolecules and, specially, proteins (in size and when loaded with drugs, metal ions or fluorophores also in function). These ultrasmall, soft nanoparticles have various applications, including catalysis, sensing, and nanomedicine. Initial in vitro experiments with nonfunctionalized, amphiphilic SCNPs loaded with a photosensitizing Zn phthalocyanine with four nonperipheral isobutylthio substituents, ZnPc, showed promise for PDT. Herein, the preparation of improved, amphiphilic SCNPs containing ZnPc as highly efficient photosensitizer encapsulated within the nanoparticle and surrounded by anthracene units is disclosed. The amount of anthracene groups and ZnPc molecules within each single-chain nanoparticle controls the imaging and PDT properties of these nanocarriers. Critically, this work opens the way to improved PDT applications based on amphiphilic SCNPs as a first step toward ideal, long-term artificial photo-oxidases (APO).

1. Introduction

Cancer is one of the most widespread diseases in the world, with an estimated 10 million deaths in 2022.[1] In recent years, in addition to the conventional medical treatment options of chemotherapy, radiotherapy and surgery and for which there are not negligible side effects,[2] much research has focused on the improving overall cancer treatment outcomes. Thus, the search for new therapeutic options such as targeted therapies, immunotherapy, hormonal therapy, gene therapy, stem cell therapy, and CAR T cells is underway.[3]

Among these different tracks, nanomedicine is a promising breakthrough in the modern era of medicine and has given new hope for the future of cancer treatment. Active ingredients are encapsulated, adsorbed, trapped or bound to nanocarriers. Nanoparticles (NP) formed in this way have shown that they can improve the administration of anti-cancer agents, particularly through selective targeting, reduced systemic toxicity and thus improved therapeutic

D. Arena, E. Verde-Sesto, A. Iturrospe, A. Arbe, J. A. Pomposo
Centro de Física de Materiales (CSIC, UPV/EHU) and Materials Physics Center MPC
Paseo Manuel Lardizabal 5, Donostia 20018, Spain
E-mail: josetxo.pomposo@ehu.eus

C. Nguyen, L. M. A. Ali, M. Gary-Bobo
Institut des Biomolécules Max Mousseron
Université de Montpellier
CNRS
ENSCM
Montpellier 34293, France
E-mail: magali.gary-bobo@inserm.fr

L. M. A. Ali
Department of Biochemistry
Medical Research Institute
University of Alexandria
Alexandria 21561, Egypt

E. Verde-Sesto, J. A. Pomposo
IKERBASQUE – Basque Foundation for Science
Plaza de Euskadi 5, Bilbao 48009, Spain

The ORCID identification number(s) for the author(s) of this article can be found under https://doi.org/10.1002/adhm.202401683

© 2024 The Author(s). Advanced Healthcare Materials published by Wiley-VCH GmbH. This is an open access article under the terms of the Creative Commons Attribution-NonCommercial-NoDerivs License, which permits use and distribution in any medium, provided the original work is properly cited, the use is non-commercial and no modifications or adaptations are made.

DOI: 10.1002/adhm.202401683

21922659, 2024, 28, Downloaded from https://advanced.onlinelibrary.wiley.com/doi/10.1002/adhm.202401683 by Acibadem Mehmet Ali Aydinlar Universitesi, Wiley Online Library on [19/03/2026]. See the Terms and Conditions (https://onlinelibrary.wiley.com/terms-and-conditions) on Wiley Online Library for rules of use; OA articles are governed by the applicable Creative Commons License

results.[4,5] For the nano-formulation there's a wide range of materials possibilities: liposomes, micelles, dendrimers, carbon nanostructures, nanoparticles, nanowires, etc. Thus in 1995, Doxil became the first liposomal nano-drug who received clinical agreement for a number of cancer treatments,[6] then Abraxane was approved by FDA as an albumin NP for the delivery of paclitaxel in breast cancer,[7] and they were successfully used in clinical practice.

Polymeric nanocarriers have emerged as a powerful tool for the delivery of tumor-targeting chemotherapeutics, allowing high entrapment efficiency, improved physiological stability, ease of surface functionalization, and manufacturing feasibility according to good manufacturing practices.[8] Polymer NPs contain the drug either in the polymer matrix or at the core of the particles and they can be loaded with hydrophobic and hydrophilic molecules, small and large molecules, proteins, and nucleic acids.[9,10] Research in polymer science has tended to focus on the development of biocompatible and biodegradable polymers to avoid induced toxicity and enhance the delivery efficacy of treatments. So, commonly used polymers for the preparation of NP are natural polymers such as collagen, alginate, chitosan, gelatin, and albumin.[11,12] but there is also many NP including synthetic polymers.

The improvement of tumor delivery efficiency thanks to nanomedicine, could also be connected to a controlled activation leading to a drug release or a cancer cell death mechanism. The stimulus could be light such as in photodynamic therapy (PDT), which is now considered as a potential treatment for solid tumors used as an alternative or complement to conventional radiotherapy and chemotherapy.[13,14] PDT is a noninvasive treatment based on the interaction between molecules called photosensitizers (PS), light stimulus at a specific wavelength adapted to the properties of the PS and molecular oxygen. The concomitance of these 3 factors will trigger the formation of reactive oxygen species (ROS) which are able to induce the tumor cell death via apoptosis or necrosis.[15] PDT will be even more effective if the PS can be delivered as close as possible to the cancer cells,[16] so NPs as carriers of PS can achieve efficient delivery of PS to tumor tissues through optimized passive targeting and ligand-modified active targeting.[17–19]

Different types of PS are developed by researchers, most of them are structural derivatives of cyclic tetrapyrroles who exhibit low or no toxicity due to their natural similarity to endogenous structures occurring in the human body (chlorophyll, heme, vitamin B12, coenzyme F430).[20–22] Among them, phthalocyanines.[23] are promising PS for PDT but their inherent tendency to aggregate generally leads to a reduction or even extinction of photoactivity. To overcome this problem and achieve the desired photodynamic therapeutic effect of phthalocyanines, encapsulation in NP seems to be an interesting solution, and obviously there are different types of encapsulation. For instance, phthalocyanine derivatives can be encapsulated into classical polymeric NPs.[24] (100 nm in diameter) or they can also enter in the composition of periodic mesoporous organosilica NP (250 nm in diameter), obtained by sol-gel condensation of a triethoxysilyl metallated phthalocyanine precursor.[25]

Single-chain nanoparticles (SCNPs) are a well-defined class of ultrasmall polymeric NP with a size corresponding to that of proteins (2–20 nm in diameter), making them suitable for biomedical applications.[26] SCNPs result through the folding of isolated synthetic polymeric chains via intrachain interactions.[27] The folding of SCNPs mimics the behavior of natural biomacromolecules and is highly desirable for a variety of applications ranging from catalysis and sensing to nanomedicine.[28–30] For instance, very recently, some of us reported the construction of artificial photosynthases (APS) as enzyme-mimetic SCNPs with manifold visible-light photocatalytic activity for challenging "in water" organic reactions.[31] Initial experiments with nonfunctionalized amphiphilic SCNPs loaded with a photosensitizing Zn phthalocyanine with four nonperipheral isobutylthio substituents, **ZnPc**, showed promising results for PDT as revealed by in vitro experiments.[32] Herein, we report the preparation of improved, amphiphilic SCNPs containing **ZnPc** as highly efficient PS encapsulated within the nanoparticle and surrounded by anthracene units as highly efficient agents for imaging and PDT in zebrafish embryo xenografts. This could be a first step toward ideal, long-term artificial photo-oxidases (APO) (**Figure 1**).

2. Results and Discussion

2.1. Preparation of Amphiphilic SCNPs Containing ZnPc Molecules and Anthracene Units

Figure 2A shows the self-folding in water of an amphiphilic polymer precursor $\mathbf{P}_x$ composed of hydrophobic anthracene methacrylate (AnMA) and hydrophilic oligo(ethylene glycol monomethyl ether) methacrylate (OEGMA) units. The formation of noncovalent, reversible, and self-assembled SCNPs is possible in water for amphiphilic copolymeric precursors in the appropriate range of molecular weights, hydrophilic/hydrophobic monomer ratio and dilution regimes.[33,34] We synthesized three well-defined poly(OEGMA-*r*-AnMA) random copolymers containing 31, 16 and 8 mol% of anthracene units that we denoted as $\mathbf{P}_1$, $\mathbf{P}_2$ and $\mathbf{P}_3$, respectively (see Figures S1–S13 in the Supporting Information). In order to observe the formation of single-chain nanoparticles, solutions of $\mathbf{P}_1$, $\mathbf{P}_2$, and $\mathbf{P}_3$ in water, all at a polymer concentration of 5 mg mL^{-1}, were prepared by dissolving 10 mg of each copolymer in 2 mL of deionized water. The resulting solutions were left stirring in the dark and at room temperature (r.t.) for 24 h. After this time, the samples were analyzed via dynamic light scattering (DLS). The reversible self-folding of $\mathbf{P}_x$ to $\mathbf{SCNP}_x$ in aqueous media was confirmed via comparison

U. İşci, Z. Şahin
Marmara University
Faculty of Technology
Department of Metallurgical and Materials Engineering
Istanbul, Turkey
F. Dumoulin
Acıbadem Mehmet Ali Aydınlar University
Faculty of Engineering and Natural Sciences
Department of Biomedical Engineering
Istanbul, Turkey
E-mail: fabienne.dumoulin@acibadem.edu.tr
J. A. Pomposo
Departamento de Polímeros y Materiales Avanzados: Física
Química y Tecnología
University of the Basque Country (UPV/EHU)
Donostia 20800, Spain

© 2024 The Author(s). Advanced Healthcare Materials published by Wiley-VCH GmbH

21922659, 2024, 28, Downloaded from https://advanced.onlinelibrary.wiley.com/doi/10.1002/adhm.202401683 by Acibadem Mehmet Ali Aydinlar Universitesi, Wiley Online Library on [19/03/2026]. See the Terms and Conditions (https://onlinelibrary.wiley.com/terms-and-conditions) on Wiley Online Library for rules of use; OA articles are governed by the applicable Creative Commons License

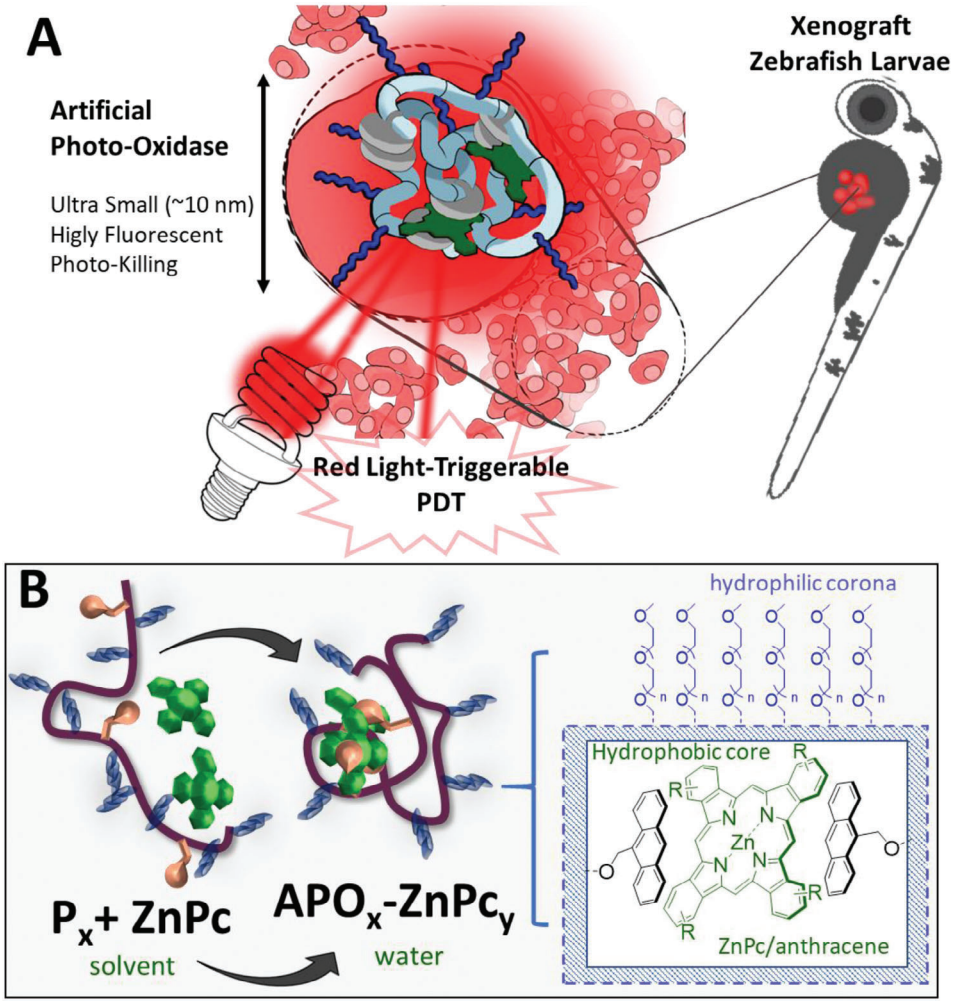

Figure 1. A) Idealized picture of an *Artificial Photo-Oxidase* (APO). B) Rational design of amphiphilic SCNPs containing a photosensitizing Zn phthalocyanine with four nonperipheral isobutylthio substituents (**ZnPc**) surrounded by anthracene ($\mathbf{P_x}$ = amphiphilic polymer precursor containing a defined amount of anthracene units; $\mathbf{APO_x\text{-}ZnPc_y}$ = SCNP prepared from $\mathbf{P_x}$ containing a defined amount of **ZnPc** encapsulated within the nanoparticle).

of the DLS size distributions of solutions of $\mathbf{P_x}$ in tetrahydrofuran (THF) and the resulting $\mathbf{SCNP_x}$ in water, both at a polymer concentration of 5 mg mL^{-1}. A reduction of the hydrodynamic diameter (D_h) of $\mathbf{P_1}$, $\mathbf{P_2}$, and $\mathbf{P_3}$ was observed when transferred to water indicating more compact structures of $\mathbf{SCNP_1}$, $\mathbf{SCNP_2}$ and $\mathbf{SCNP_3}$ with respect to those of $\mathbf{P_1}$, $\mathbf{P_2}$, and $\mathbf{P_3}$ in THF (see Figure 2B). Concomitantly, the slight bathochromic shift of the UV–visible absorbance in the range between 300 and 400 nm (see Figure 2C and Figures S14–S16, Supporting Information), as well as the pronounced decrease in fluorescence intensity, broadening of the emission band and its red-shifting (see Figure 2D) are indicative of self-aggregation, similar to that reported for anthracene solid-state phenomena such as excimer formation.[35] Additional evidence of anthracene self-aggregation was obtained by ^{1}H nuclear magnetic resonance (NMR) spectroscopy showing changes in the chemical shifts of the aromatic and benzylic protons of $\mathbf{SCNP_1}$, $\mathbf{SCNP_2}$, and $\mathbf{SCNP_3}$ (Figure S1, Supporting Information).

Having demonstrated the self-folding ability of $\mathbf{P_x}$ in water to give $\mathbf{SCNP_x}$, we envisioned the construction of improved, amphiphilic SCNPs containing a photosensitizing Zn phthalocyanine with four nonperipheral isobutylthio substituents, **ZnPc** (Figure S17, Supporting Information), encapsulated within $\mathbf{SCNP_x}$ as highly efficient photosensitizer (PS) surrounded by anthracene units as highly efficient nanocarriers for PDT applications.[36] Moreover, we surmised that the presence of **ZnPc** would endow the resulting SCNPs with useful imaging properties. For the preparation, we selected an overall $\mathbf{P_x}$ concentration in solution of 5 mg mL^{-1}. Under these conditions, $\mathbf{P_1}$, $\mathbf{P_2}$, and $\mathbf{P_3}$ allowed the preparation of different single-chain nanoparticles charged with the photoactive **ZnPc** at three different loadings that we denote as $\mathbf{APO_1\text{-}ZnP_{60}}$, $\mathbf{APO_2\text{-}ZnP_{25}}$, and $\mathbf{APO_3\text{-}ZnP_{10}}$, corresponding to overall **ZnPc** concentrations in solution of 60, 25, and 10×10^{-6} M respectively. As a general procedure for encapsulation of the **ZnPc** (see **Figure** 3A), 25 mg of the copolymer nanocarrier were weighted in an amber glass vial and diluted with 100 µL of inhibitor-free THF. After stirring at r.t. for 1 h, *n* µL of **ZnPc** stock solution (1 g L^{-1} in inhibitor-free THF) was added to the solution, with *n* selected depending on the desired final concentration of **ZnPc**. The resulting solution

© 2024 The Author(s). Advanced Healthcare Materials published by Wiley-VCH GmbH

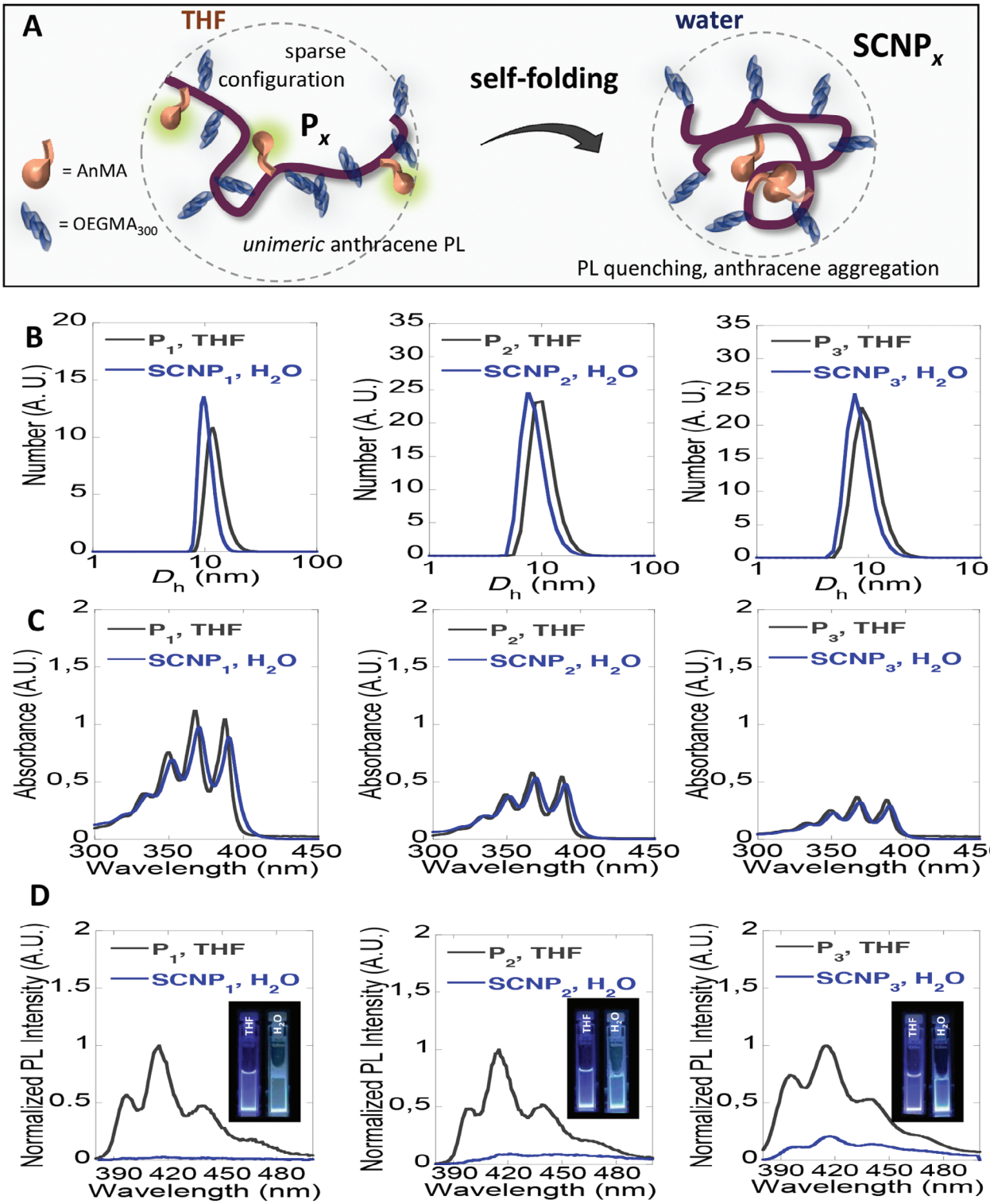

Figure 2. A) Depiction of the self-folding of an anthracene-containing amphiphilic precursor, $\mathbf{P_x}$, which presents typical anthracene photoluminescence (PL) when in open-chain conformation in THF (*good solvent* for both AnMA and OEGMA), to the self-assembled SCNP in water (*selective solvent* for OEGMA) in which the anthracene PL is lost due to self-aggregation. B) DLS size distributions of copolymers $\mathbf{P_1}$ (anthracene content: 31 mol%), $\mathbf{P_2}$ (16 mol%) and $\mathbf{P_3}$ (8 mol%) showed as superimposed populations measured in THF and water (in the latter case as $\mathbf{SCNP_1}$, $\mathbf{SCNP_2}$ and $\mathbf{SCNP_3}$, respectively) [copolymer] = 5 mg mL^{-1}. C) UV-Vis absorbance spectra of $\mathbf{P_1}$, $\mathbf{P_2}$ and $\mathbf{P_3}$ in THF and $\mathbf{SCNP_1}$, $\mathbf{SCNP_2}$ and $\mathbf{SCNP_3}$ in water, [copolymer] = 0.2 mg mL^{-1} (see Figures S14–S16 in the Supporting Information for [copolymer] = 0.1 mg mL^{-1}). D) PL emission spectra of $\mathbf{P_1}$, $\mathbf{P_2}$, and $\mathbf{P_3}$ in THF and $\mathbf{SCNP_1}$, $\mathbf{SCNP_2}$ and $\mathbf{SCNP_3}$ in water, [copolymer] = 0.2 mg mL^{-1}. Insets show naked-eye reduction of anthracene photoluminescence after self-assembly in water.

© 2024 The Author(s). Advanced Healthcare Materials published by Wiley-VCH GmbH

21922659, 2024, 28, Downloaded from https://advanced.onlinelibrary.wiley.com/doi/10.1002/adhm.202401683 by Acibadem Mehmet Ali Aydinlar Universitesi, Wiley Online Library on [19/03/2026]. See the Terms and Conditions (https://onlinelibrary.wiley.com/terms-and-conditions) on Wiley Online Library for rules of use; OA articles are governed by the applicable Creative Commons License

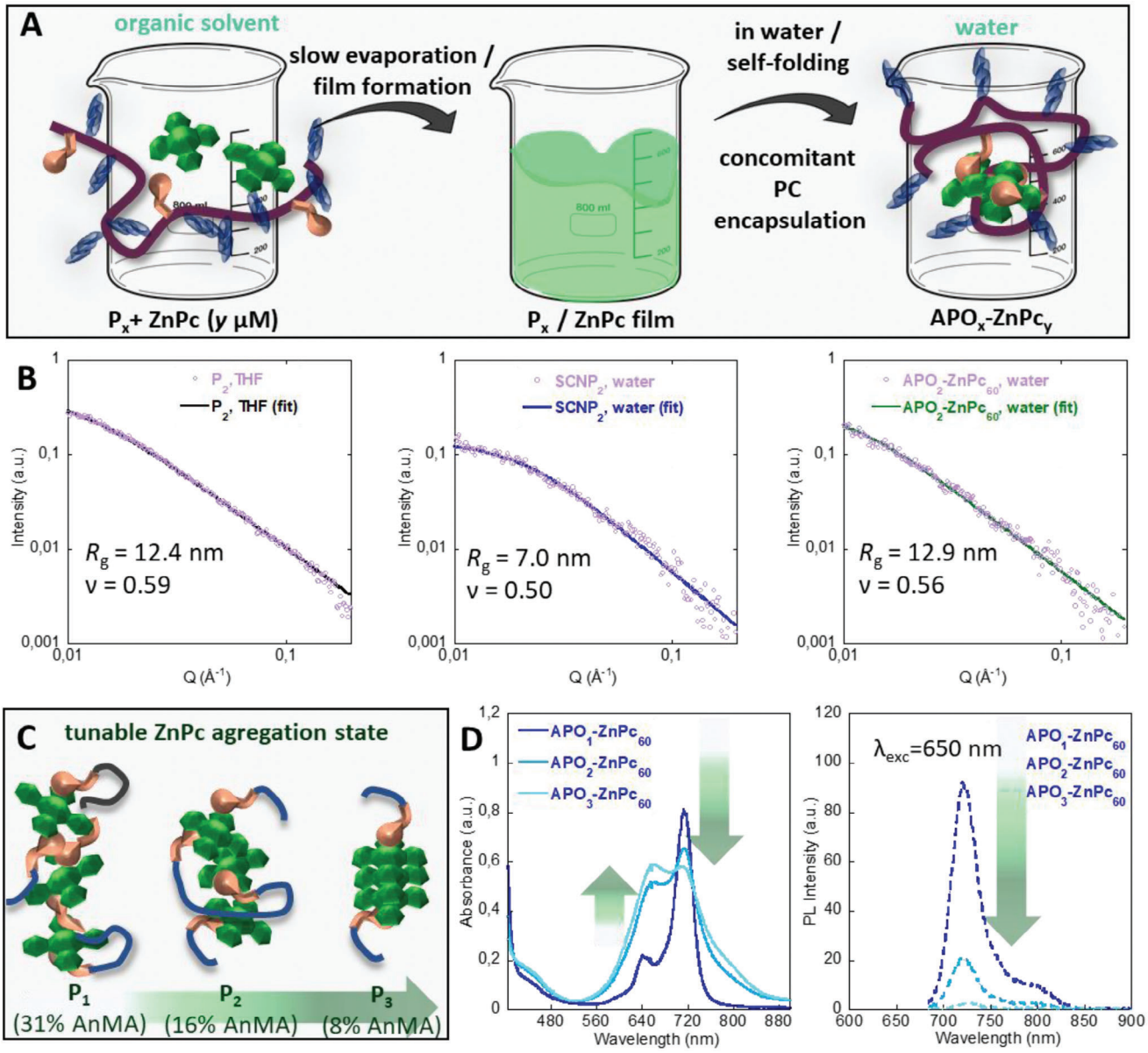

Figure 3. A) Schematic illustration of the synthetic procedure followed for the formation of self-assembled **APO$_x$-ZnPc$_y$**. B) Small-angle X-ray scattering (SAXS) results (R_g is the radius of gyration, ν is the scaling exponent) revealing the compaction of **P$_2$** switching solvents from THF to water (**SCNP$_2$**), followed by an enlargement of the radius of gyration (R_g) upon **ZnPc** incorporation within the nanoparticle to give **APO$_2$-ZnPc$_{60}$**. C) Idealized picture showing the tuning of the aggregation state of the **ZnPc** encapsulated within the core of the SCNP depending on the anthracene content in the precursor. D) On the left, UV-Vis spectra of **APO$_1$-ZnPc$_{60}$**, **APO$_2$-ZnPc$_{60}$** and **APO$_3$-ZnPc$_{60}$** in water ([copolymer] = 1 mg mL^{-1}). On the right, PL emission spectra of the same solutions, recorded after oxygen displacement by argon bubbling.

was left stirring at r.t. and in the dark for 72 h to ensure complete evaporation of the organic solvent. After this time, 5 mL of deionized water was added to the resulting polymeric film and the final mixture was left under gentle agitation at r.t. and in the dark for 24 h. The resulting clear and transparent solutions of **APO$_x$-ZnPc$_y$** were analyzed via small-angle X-ray scattering (see Figure 3B) and stored in a dark place at 4 °C. Considering the strong hydrophobicity of the phthalocyanine used in this work, we assumed that the total absence of any precipitate in solution (confirmed by the absence of aggregates in DLS experiments) is a good indication of a quantitative encapsulation of **ZnPc** within the hydrophobic core of the SCNP. A further confirmation was obtained by the comparison of the radius of gyration (R_g) of the single-chain nanoparticles in water *prior*- and *post*-encapsulation of the **ZnPc** (Figure 3B). After encapsulation, the values of R_g were always higher with respect to the neat (**ZnPc** free) nanocarriers, which we attribute to the increased steric hindrance in the core of the nanoparticles, due to the encapsulated **ZnPc**. TEM revealed the globular morphology of the **APO$_x$-ZnPc$_y$** in the dry state (Figure S18, Supporting Information). Very good synthesis

© 2024 The Author(s). Advanced Healthcare Materials published by Wiley-VCH GmbH

21922659, 2024, 28, Downloaded from https://advanced.onlinelibrary.wiley.com/doi/10.1002/adhm.202401683 by Acibadem Mehmet Ali Aydinlar Universitesi, Wiley Online Library on [19/03/2026]. See the Terms and Conditions (https://onlinelibrary.wiley.com/terms-and-conditions) on Wiley Online Library for rules of use; OA articles are governed by the applicable Creative Commons License

reproducibility of **APO$_x$-ZnPc$_y$** was observed from batch to batch (Figure S19, Supporting Information).

We hypothesized that changes in the anthracene content in the SCNPs could have significant effects in its photophysical properties (see Figure 3C). As illustrated in Figure 3D, by measuring the UV–Vis absorbance of the **APO$_x$-ZnPc$_y$** we observed a clear correlation between the molar fraction of anthracene units in the nanocarrier and the aggregation degree of the encapsulated phthalocyanine PS. As shown in Figure 3D-left by the comparison of the absorption in the far-red region of **APO$_1$-ZnPc$_{60}$**, **APO$_2$-ZnPc$_{60}$** and **APO$_3$-ZnPc$_{60}$**, the extent of either broadening or quenching of Q-band transitions increases upon decreasing the anthracene molar fraction in the nanocarrier. Analogously, a pronounced quenching (λ^{exc} = 650 nm) of the **ZnPc** emission in the far red is observed upon decreasing the anthracene content from 31 mol% (**APO$_1$-ZnPc$_{60}$**) to 8 mol% (**APO$_3$-ZnPc$_{60}$**) (see Figure 3D-right and Figure S20, Supporting Information). Consequently, this novel class of amphiphilic SCNPs not only enables the facile encapsulation of the far-red absorbing **ZnPc**, but also allows the tunability of the degree of aggregation within the hydrophobic core of the nanocarrier.

2.2. In Vitro Imaging and PDT with Amphiphilic SCNPs Containing ZnPc Molecules and Anthracene Units

To determine the therapeutic potential of the **APO$_x$-ZnPc$_y$**, we first assessed their intrinsic toxicity by means of performing cytotoxicity experiments against human breast adenocarcinoma (MDA-MB-231) cells. In a typical experiment, the cytotoxicity against MDA-MB-231 cells was estimated after having incubated the cells with the **APO$_x$-ZnPc$_y$** at fixed concentrations for 72 h using the 3-(4,5-dimethyltriazol-2-yl)−2,5-diphenyltetrazolium bromide (MTT) test.[37] **Figure 4** shows that no significant cytotoxic activity was observed when MDA-MB-231 cells were incubated in presence of **APO$_x$-ZnPc$_y$** at a nanoparticle concentration of up to 100 μg mL^{-1}. The good biocompatibility observed for this novel class of nanocarriers is, after all, in agreement with what reported for other PEGylated nanoparticles employed in nanomedicine applications.[38]

Next, we explored the cellular uptake of **APO$_x$-ZnPc$_y$** by MDA-MB-231 cells. For these experiments, we selected the SCNPs with the higher **ZnPc** content, **APO$_x$-ZnPc$_{60}$**, as the internalization was visualized by fluorescence microscopy exploiting the intrinsic fluorescence ($\lambda^{exc}{}_{max}$ = 630 nm) of the encapsulated phthalocyanine. As shown in **Figure 5A**, long-wavelength emitted photoluminescence (PL) of the photosensitizer **ZnPc** was observed for all the three SCNP-based nanosystems. Notably, the fluorescence intensity relations measured in aqueous solutions of **APO$_x$-ZnPc$_{60}$** (Figure 2D), specifically **APO$_1$-ZnPc$_{60}$** > **APO$_2$-ZnPc$_{60}$** ≈ **APO$_3$-ZnPc$_{60}$**, was qualitatively maintained also upon internalization in MDA-MB-231 cells. Conversely, when MDA-MB-231 cells were incubated with nonencapsulated **ZnPc** under the same experimental conditions, no substantial internalization was observed. Consequently, encapsulation of the highly hydrophobic and self-aggregating **ZnPc** within the APO is essential for ensuring good bioavailability. Figure 5B shows that **APO$_2$-ZnPc$_{60}$** was efficiently internalized by MDA-MB-231 cancer cells.

Then, the PDT effect in cancer cells was investigated at two different irradiation wavelengths in the far-red region of the visible spectrum of light, namely at $\lambda_{exc}{}^{max}$ = 630 nm and $\lambda_{exc}{}^{max}$ = 730 nm. MDA-MB-231 cells were incubated for 24 h with the **APO$_x$-ZnPc$_y$** at an optimal concentration of 100 μg mL^{-1}, since performing the same experiments at lower SCNPs contents (25 μg mL^{-1}) resulted in a less remarkable effect. Notably, all the samples showed PDT-effect when a 630 nm light source was employed for irradiation (**Figure 6A**). All **APO$_x$-ZnPc$_{60}$** manifested high cell photokilling ability, with the specific PDT effect of **APO$_2$-ZnPc$_{60}$** being tremendous. Interestingly, significant PDT-effect was observed when shifting to the longer irradiation wavelength (730 nm) (Figure 6B). To further test the suitability of **APO$_x$-ZnPc$_{60}$** nanoparticles as effective PDT agents, we performed the same experiments exposing the 96-well plate at room light for 3 h, and no cytotoxicity was observed (see Figure S21 in the Supporting Information). These results indicate that the confinement of the **ZnPc** within the core of the **APO$_x$-ZnPc$_y$** yields nanoaggregates with a PDT activity which is selective for long-wavelength and intense radiations, a highly desirable quality for perspective application in more complex systems.

We confirmed that the cell-killing activity of **APO$_x$-ZnPc$_y$** is due to a PDT mechanism by demonstrating the in vitro ROS production during light excitation. Hence, cells were incubated with the nonfluorescent reactant 2′,7′-dichlorodihydrofluorescein diacetate (DCFH-DA) for 45 min. In the presence of ROS, the molecule is straightforwardly oxidized to its fluorescent form 2′,7′-dichlorofluorescein (DCF), whose characteristic intense green luminescence was detected by fluorescence microscopy.[39] The results shown in Figure 6C illustrate that, when incubated for 24 h in presence of 100 μg mL^{-1} of **APO$_x$-ZnPc$_y$**, light excitation at a maximum wavelength of 630 nm induced green fluorescence inside the tumor cells. This result qualitatively demonstrates intracellular ROS production and confirms that the cell death follows a PDT-like mechanistic pathway.

2.3. Amphiphilic SCNPs Containing ZnPc Molecules and Anthracene Units as Imaging and Far-Red Photokilling Agents for PDT in Zebrafish Embryo Xenografts

With the biomedical potential of **APO$_x$-ZnPc$_y$** for PDT assessed, we wanted to further demonstrate their employability by performing both fluorescence imaging and PDT experiments in zebrafish embryos as integrated models for human tumor.[40] (**Figure 7A**). First, we assessed the **APO$_x$-ZnPc$_y$** capability to induce long-wavelength fluorescence in zebrafish larvae. Specifically, we injected 72 h post fertilization (hpf) zebrafish embryos with **APO$_x$-ZnPc$_y$** from the three different copolymer precursors **P$_1$**, **P$_2$**, and **P$_3$** at their highest **ZnPc**-loading (**APO$_x$-ZnPc$_{60}$**), which were administrated through intravenous (IV) injection (Figure 7B). After letting circulate the nanoparticles in the organisms' bloodstreams for 4 h, we captured the photoluminescence by fluorescence microscopy using a maximum excitation wavelength of 630 nm. As shown in Figure 7C, the **APO$_x$-ZnPc$_y$** easily and homogeneously distributed in the vas-

© 2024 The Author(s). Advanced Healthcare Materials published by Wiley-VCH GmbH

21922659, 2024, 28, Downloaded from https://advanced.onlinelibrary.wiley.com/doi/10.1002/adhm.202401683 by Acibadem Mehmet Ali Aydinlar Universitesi, Wiley Online Library on [19/03/2026]. See the Terms and Conditions (https://onlinelibrary.wiley.com/terms-and-conditions) on Wiley Online Library for rules of use; OA articles are governed by the applicable Creative Commons License

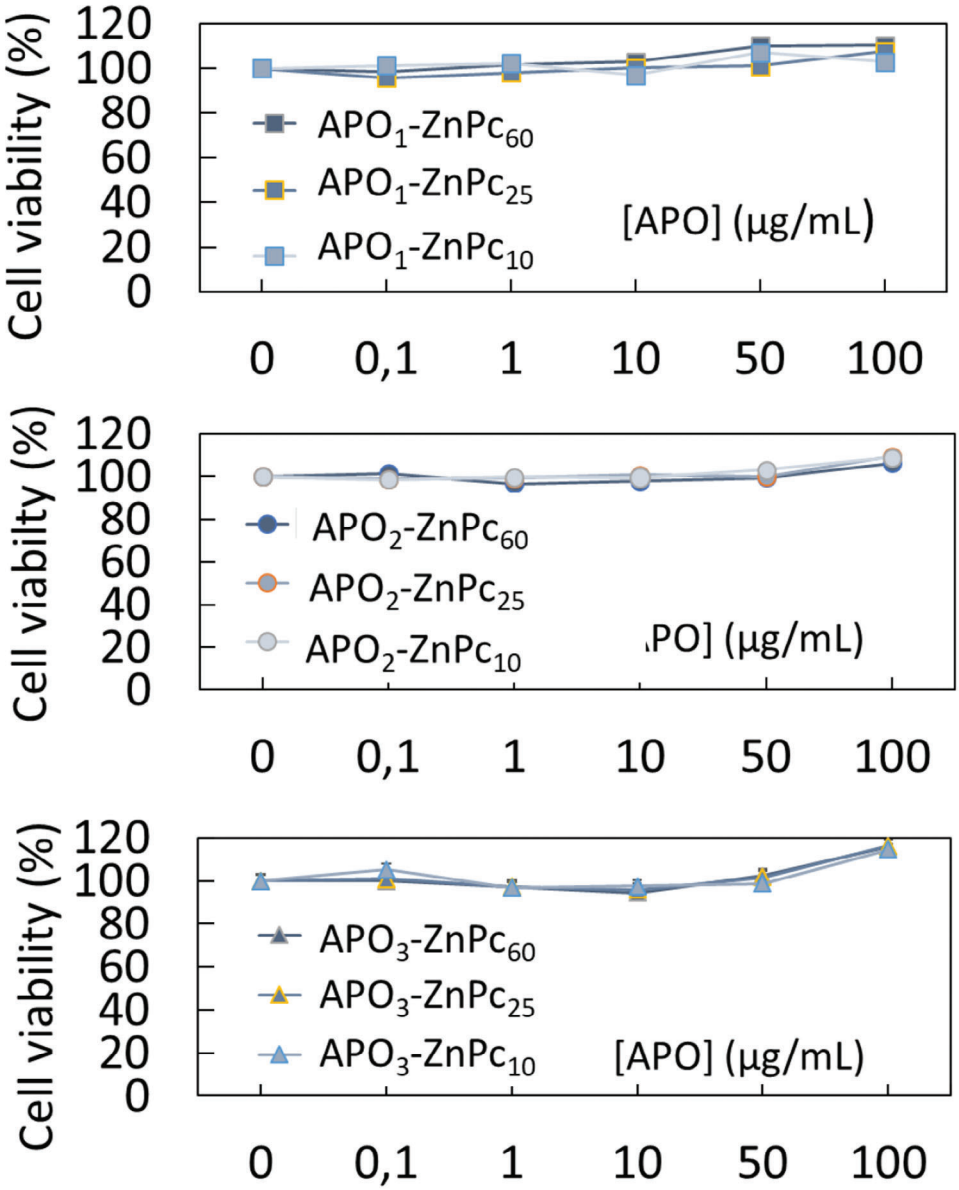

Figure 4. Dark cytotoxicity experiments of **APO_x-$ZnPc_y$** against human breast adenocarcinoma MDA-MB-231 cells, which were incubated 72 h with increasing concentrations of **APO_x-$ZnPc_y$**. Values are means ± standard deviations of 3 experiments.

cular system of the subjects, indicating both a good biodistribution behavior and appropriate properties of the amphiphilic SCNPs also in the chemically complex zebrafish larvae's vascular system. Interestingly, analogous PL intensity patterns (**APO_1-$ZnPc_{60}$** > **APO_2-$ZnPc_{60}$** ~ **APO_3-$ZnPc_{60}$**), already observed for in vitro experiments, were observed also upon injection in the embryos. Encouraged by all the above-mentioned results, we finally carried out PDT experiments on zebrafish larvae Xenografts to further evaluate the potential of this novel class of ultrasmall nanoparticles for PDT cancer treatment. For this, we first seeded MDA-MB-231 cells expressing the fluorescent protein Luciferase (RFP) with the nanoparticles which shown the best in vitro results, namely **APO_2-$ZnPc_{60}$** solutions, at a polymer concentration of 100 µg mL^{-1} for an incubation time of 24 h. After **APO_2-$ZnPc_{60}$** internalization, culture media were rinsed and concentrated up to reach a cell concentration suitable for intra-yolk injection (see Experimental Section for the detailed procedure). 72 hpf zebrafish embryos were then injected with **APO_2-$ZnPc_{60}$**-loaded (or not loaded) MDA-MB-231 Luc RFP cells via injection in the yolk, ensuring an injection of about 200–400 cells per subject. After a period of 24 h for tumor implantation, fluorescence microscopy images of all the tumors were recorded exploiting the RFP-responding luminescence of the Luciferase expressed by the tumor cells and the subjects were (or not) subsequently exposed to light irradiation (λ^{exc}_{max} = 630 nm) for a total duration of 10 min. using the same microscope. 24 h after the irradiation, images of the tumors were captured again and under the same optical condi-

© 2024 The Author(s). Advanced Healthcare Materials published by Wiley-VCH GmbH

21922639, 2024, 28, Downloaded from https://advanced.onlinelibrary.wiley.com/doi/10.1002/adhm.202401683 by Acibadem Mehmet Ali Aydinlar Universitesi, Wiley Online Library on [19/03/2026]. See the Terms and Conditions (https://onlinelibrary.wiley.com/terms-and-conditions) on Wiley Online Library for rules of use; OA articles are governed by the applicable Creative Commons License

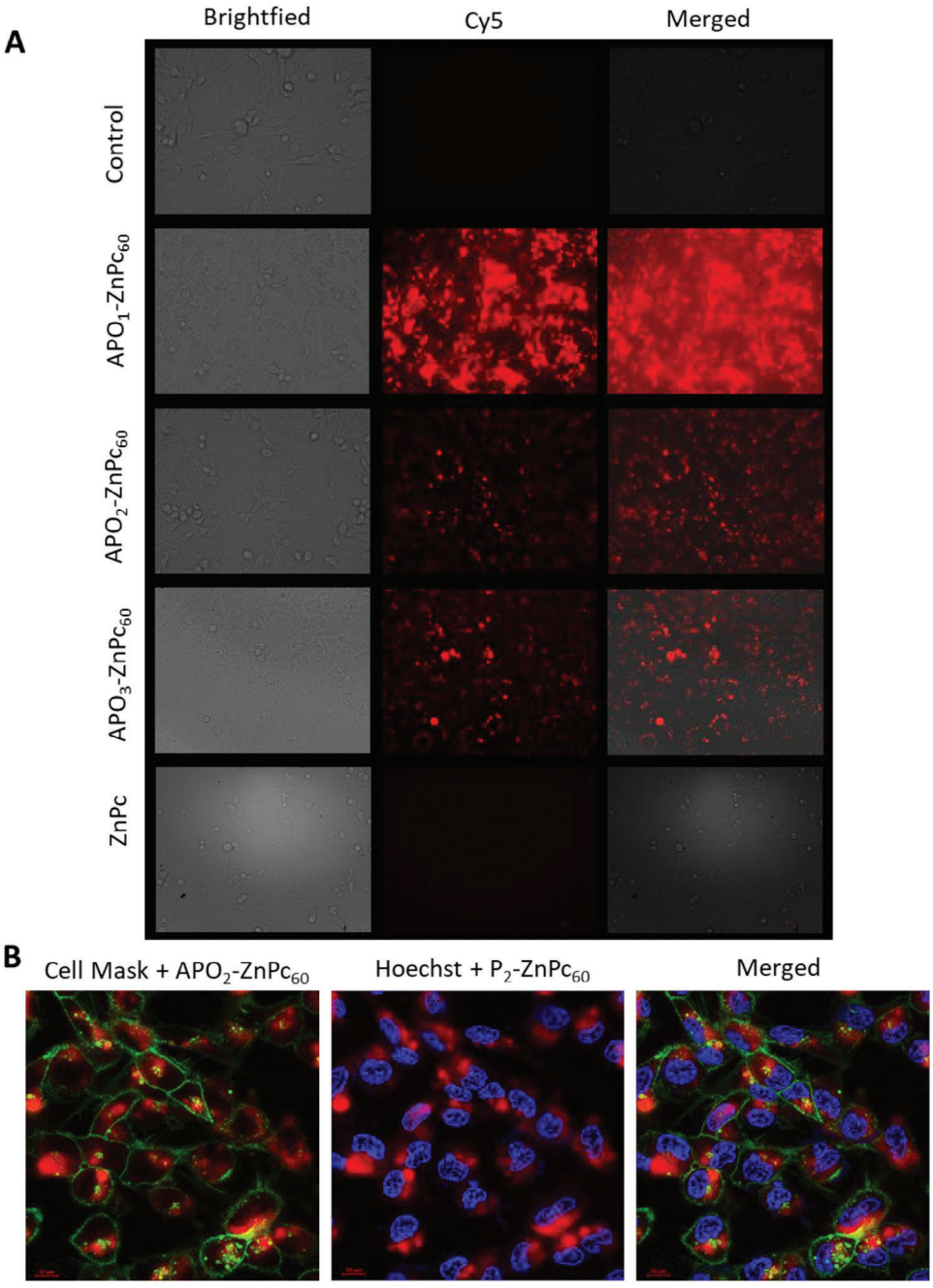

Figure 5. A) Fluorescence microscopy images recorded on MDA-MB-231 breast cancer cells treated either (or not) with **APO_x-$ZnPc_{60}$** at 100 µg mL^{-1} or with nonencapsulated **ZnPc** (1.2×10^{-6} M). The fluorescence of **APO_x-$ZnPc_{60}$** is revealed using an excitation wavelength of 630 nm. B) Confocal microscopy images of MDA-MB-231 breast cancer cells incubated with **APO_2-$ZnPc_{60}$**, 100 µg mL^{-1}. Cell membranes and nuclei stained with Cell Mask (green) and Hoechst (blue), respectively.

tions, allowing to follow the evolution of the extent of the tumoral mass in each specific and different experimental condition (Figure 7D). The resulting graphical representation, which was built with six individual subjects for each condition is illustrated in Figure 7E, and suggest that **APO_2-$ZnPc_{60}$** shows a promising photokilling effect against human cancer cells in zebrafish larvae xenografts. While in either nontreated or treated but not irradiated subjects the tumor fluorescence showed a neat increase with respect to initial conditions, in the case of irradiated and treated ones an encouraging diminishment of tumor size was found of 36% decrease in comparison to non irradiated embryos.

© 2024 The Author(s). Advanced Healthcare Materials published by Wiley-VCH GmbH

21922659, 2024, 28, Downloaded from https://advanced.onlinelibrary.wiley.com/doi/10.1002/adhm.202401683 by Aciibadem Mehmet Ali Aydinlar Universitesi, Wiley Online Library on [19/03/2026]. See the Terms and Conditions (https://onlinelibrary.wiley.com/terms-and-conditions) on Wiley Online Library for rules of use; OA articles are governed by the applicable Creative Commons License

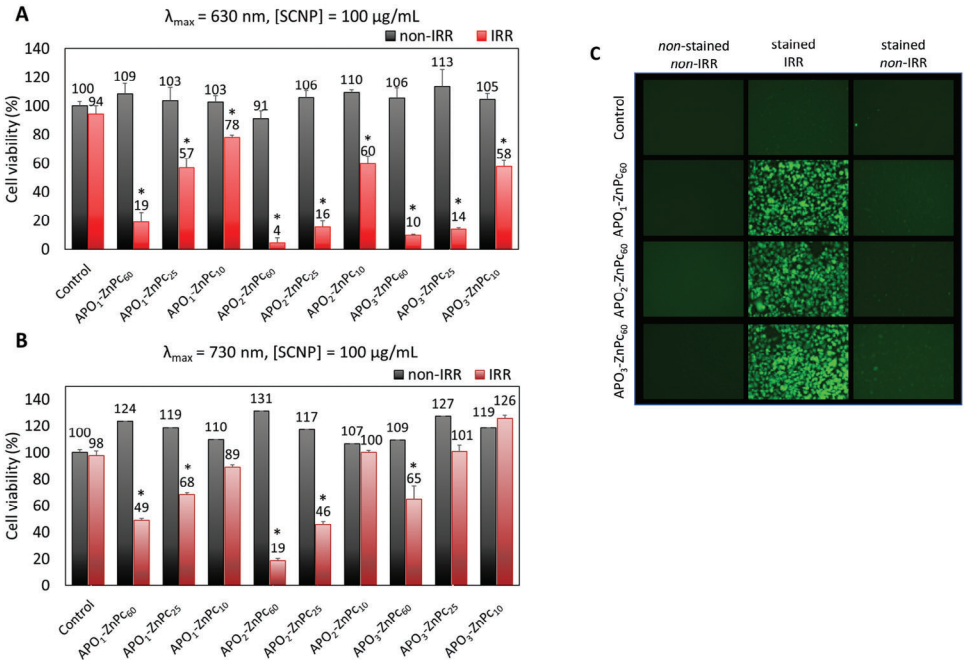

Figure 6. PDT-effect studies of **APO_x-$ZnPc_y$** incubated in MDA-MB-231 cells using an irradiation wavelength of 630 nm A) or 730 nm B). Values are means ± standard deviations of 3 experiments. *, p-value < 0.05, significantly different between non-IRR and IRR. C) Detection of intracellular ROS in MDA-MB-231 cells incubated for 24 h with 100 µg mL^{-1} of **APO_x-$ZnPc_{60}$** and 20 × 10^{-6} M DCFDA for 45 min and irradiated with a 630 nm light source. Green fluorescence was observed under GFP filter (λ_{exc} = 480 nm).

3. Conclusion

In conclusion, highly efficient nanocarriers for photodynamic therapy (PDT) result through the encapsulation of a photosensitizing Zn phthalocyanine with four nonperipheral isobutylthio substituents, **ZnPc**, within amphiphilic single-chain nanoparticles (SCNPs) containing hydrophobic anthracene pendants. The imaging and PDT properties of the resulting **APO_x-$ZnPc_y$** nanocarriers are readily tunable by adjusting both the amount of anthracene units and **ZnPc** molecules within each single-chain nanoparticle. All **APO_x-$ZnPc_y$** showed excellent biocompatibility as revealed by dark cytotoxicity experiments as well as potent PDT properties inside human breast adenocarcinoma (MDA-MB-231) cells when irradiated at 630 or 730 nm. In particular, **APO_2-$ZnPc_{60}$** shows a promising photokilling effect against human tumor cells in zebrafish larvae xenografts. This work is a first step toward the long-term development of innovative artificial photooxidases for biomedical applications.

4. Experimental Section

Materials: Unless otherwise noted, all reagents and solvents were used as received from vendors. Oligo(ethylene glycol monomethyl ether) methacrylate (OEGMA, average molecular weight = 300 Da) (>99%) was purchased from TCI Europe N.V. and was filtered over basic alumina before use. *n*-Hexane (96%), was purchased from Scharlab. Tetrahydrofuran (THF) (>99%, + 0.025% BHT as stabilizer), ethanol (EtOH) (>99%) and methanol (MeOH) (>99%) were purchased from Fisher Scientific. Inhibitor-free THF was obtained by filtration of THF (Fisher Scientific) over basic alumina. 1,4-Dioxane (>99%), 9-anthracenylmethyl methacrylate (>99%), 4-cyano-4-(phenylcarbonothioylthio)pentanoic acid (CPADB) and dimethyl sulfoxide (98%) were purchased from Sigma-Aldrich. Azobisisobutyronitrile (AIBN) (98%) was purchased from Fluka and recrystallized from MeOH prior use. Basic alumina (0.063-0.2 mm) was purchased from Merck. Deuterated chloroform ($CDCl_3$, 99.8% D, + 0.03% tretramethylsilane) for ^{1}H NMR analysis was purchased from Eurisotop. Deionized water was obtained from a Thermoscientific Barnstead TII System.

Synthesis of the Photosensitizer ZnPc: The preparation of the nonperipheral tetrakis(isobutylthio) Zn phthalocyanine, **ZnPc**, was carried out as reported elsewhere.[32] (its chemical structure is depicted in Figure S17 in the Supporting Information).

Preparation of the Amphiphilic Copolymers. Synthesis of P_1: 177 mg (0.64 mmol) of 9-anthracenylmethyl methacrylate (AnMA), 450 mg (1.5 mmol) of oligo(ethylene glycol monomethyl ether) methacrylate (OEGMA), 1.51 mg (5.4 µmol) of 4-cyano-4-(phenylcarbonothioylthio)pentanoic acid (CPADB), 0.34 mg (2.1 µmol) of azobisisobutyronitrile (AIBN) and 1.07 mL of 1,4-dioxane were added to a dark, oven-dried vial, equipped of a magnetic stir bar. After purging the mixture with an argon flow for 10 min., the vial was sealed with a rubber septum, and the reaction was left stirring at 70 °C and under inert atmosphere for 19 h. After this time, the crude was purified via four consecutive precipitations in *n*-hexane. After drying under dynamic vacuum for 24 h, the obtained product was analyzed via size exclusion chromatography (SEC) and NMR. M_w (kDa) = 184.5, $Đ$ = 1.39, AnMA (mol%) = 31. ^{1}H NMR (400 MHz, $CDCl_3$): δ (ppm) = 8.44-7.42 (m, 9H, H^{Ar}), 5.98 (b.s., 2H, $H_9C_{10}CH_2$), 4.08-3.99 (m, 2H, CH_2CH_2O), 3.62–3.50, (m, $(OCH_2CH_2)_n$), 3.34 (s, 3H, OCH_3), 1.74 (m, CH_2CCH_3), 1-0.83 (m, CH_2CCH_3).

Synthesis of P_2: 98 mg (0.35 mmol) of AnMA, 600 mg (2 mmol) of OEGMA, 1.65 mg (5.9 µmol) of CPADB, 0.39 mg (2.4 µmol) of AIBN and 1.07 ml of 1,4-dioxane were added to a dark, oven-dried vial, equipped of a magnetic stir bar. After purging the mixture with an argon flow for 10 minutes, the vial was sealed with a rubber septum, and the reaction was left stirring at 70 °C and under inert atmosphere for 19 h. After this time, the crude was purified via four consecutive precipitations in *n*-

© 2024 The Author(s). Advanced Healthcare Materials published by Wiley-VCH GmbH

21922659, 2024, 28, Downloaded from https://advanced.onlinelibrary.wiley.com/doi/10.1002/adhm.202401683 by Acibadem Mehmet Ali Aydinlar Universitesi, Wiley Online Library on [19/03/2026]. See the Terms and Conditions (https://onlinelibrary.wiley.com/terms-and-conditions) on Wiley Online Library for rules of use; OA articles are governed by the applicable Creative Commons License

21922659, 2024, 28, Downloaded from https://advanced.onlinelibrary.wiley.com/doi/10.1002/adhm.202401683 by Acibadem Mehmet Ali Aydinlar Universitesi, Wiley Online Library on [19/03/2026]. See the Terms and Conditions (https://onlinelibrary.wiley.com/terms-and-conditions) on Wiley Online Library for rules of use; OA articles are governed by the applicable Creative Commons License

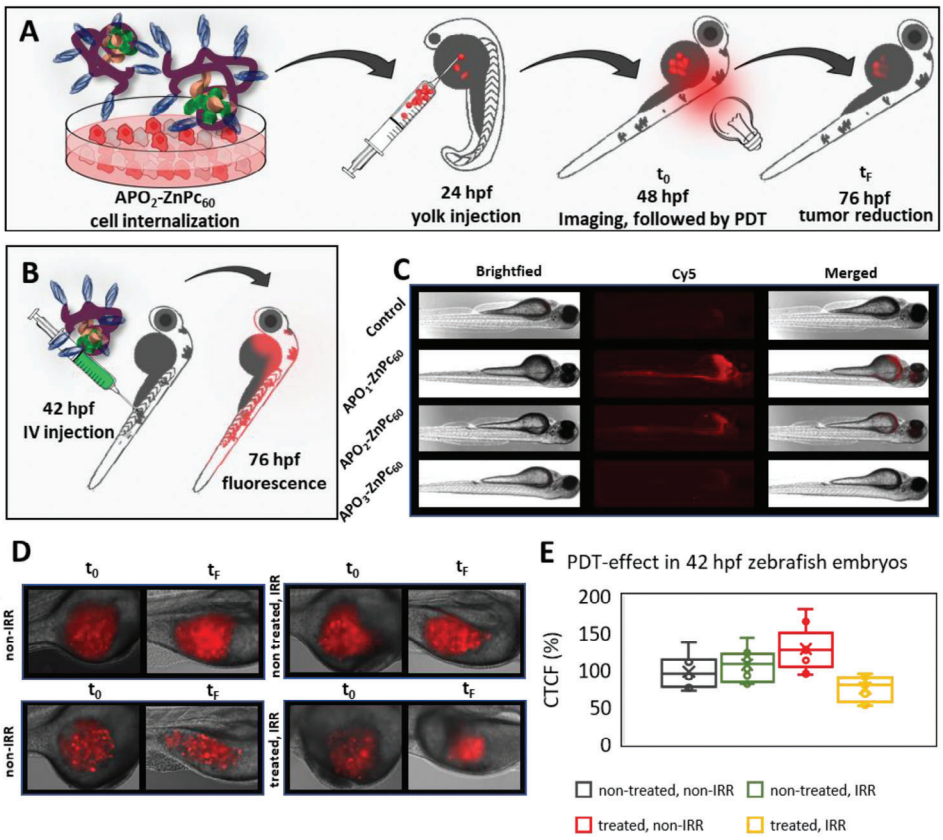

Figure 7. A) Scheme of the PDT experiment of xenograft zebrafish embryos tumor model. B) Scheme of the **APO_x-$ZnPc_{60}$**-induced fluorescence in the zebrafish. C) Experimental results of **APO_x-$ZnPc_{60}$**-induced fluorescence in zebrafish. D) Fluorescence microscopy imaging of four representative cases, one for each experimental condition explored, of the PDT effect of **APO_2-$ZnPc_{60}$** in zebrafish embryos (t_0 = image captured before tumor irradiation, t_F = image captured 24 h after irradiation (or not). E) PDT effect of **APO_2-$ZnPc_{60}$** on human tumors (MDA-MB-231) xenografted on zebrafish embryos and irradiated (or not) 10 min at 630 nm, $n = 6$ embryos per condition.

hexane. After drying under dynamic vacuum for 24 h, the obtained product was analyzed via SEC and NMR. M_w (kDa) = 157.1, $Đ$ = 1.20, AnMA (mol%) = 16. ^{1}H NMR (400 MHz, $CDCl_3$): δ (ppm) = 8.5–7.51 (m, 9H, H^{Ar}), 6.02 (b.s., 2H, $H_9C_{10}\underline{CH_2}$), 4.07 (m, 2H, $CH_2\underline{CH_2}O$), 4.00–3.53, (m, $(OCH_2CH_2)_n$), 3.36 (s, 3H, $O\underline{CH_3}$), 1.88 (m, $C\underline{H_2}CCH_3$), 1.01–0.84 (m, $CH_2CC\underline{H_3}$).

Synthesis of P_3: 49 mg (0.175 mmol) of AnMA, 600 mg (2 mmol) of OEGMA, 3.3 mg (11.8 µmol) of CPADB, 0.78 mg (4.8 µmol) of AIBN and 1.07 mL of 1,4-dioxane were added to a dark, oven-dried vial, equipped of a magnetic stir bar. After purging the mixture with an argon flow for 10 min., the vial was sealed with a rubber septum, and the reaction was left stirring at 70 °C and under inert atmosphere for 19 h. After this time, the crude was purified via four consecutive precipitations in *n*-hexane. After drying under dynamic vacuum for 24 h, the obtained product was analyzed via SEC and NMR. M_w (kDa) = 132.7, $Đ$ = 1.23,% AnMA (mol%) = 8%. ^{1}H NMR (400 MHz, $CDCl_3$): δ (ppm) = 8.53–7.52 (m, 9H, H^{Ar}), 6.03 (b.s., 2H, $H_9C_{10}\underline{CH_2}$), 4.08 (m, 2H, $CH_2\underline{CH_2}O$), 3.74–3.54, (m, $(OCH_2CH_2)_n$), 3.37 (s, 3H, $O\underline{CH_3}$), 1.85 (m, $C\underline{H_2}CCH_3$), 1.26–0.88 (m, $CH_2CC\underline{H_3}$).

Preparation of APO_x-$ZnPc_y$: As a general procedure for encapsulation of **ZnPc**, 25 mg of **P_x** was weighted in an amber glass vial and diluted with 100 µL of inhibitor-free THF. After stirring at room temperature for 1 h, *n* µL of a **ZnPc** stock solution (1 g L^{-1} in inhibitor-free THF) was added to the solution, with *n* selected depending on the desired final *y* µM concentration of **ZnPc**. The resulting solution was left stirring at r.t. and in the dark for 72 h to ensure complete evaporation of the organic solvent. After this time, 5 mL of deionized water was added to the resulting polymeric film, and the final mixture was left under gentle agitation at r.t. and in the dark for 24 h. The resulting clear and transparent **APO_x-$ZnPc_y$** solutions were analyzed via DLS and UV–vis spectrometry, and finally stored in a dark place at 4 °C.

Cell Culture Conditions for In Vitro Experiments: Human breast adenocarcinoma MDA-MB-231, the standard cell line or this expressing luciferase and red fluorescent protein (MDA-MB-231 Luc RFP) were purchased from ATCC (American Type Culture Collection, Manassas, VA). Cells were cultured in Dulbecco's Modified Eagle's Medium (DMEM), incorporating 10% Fetal Bovine Serum and antibiotic (FBS) (2% penicillin–streptomycin). MDA-MB-231 Luc RFP cells were maintained in the previously mentioned cell culture medium copositions in addition to 5 µg mL^{-1} blasticidin as a selection antibiotic. The cell growth was performed in humidified atmosphere at 37 °C under 5% CO_2. DMEM, FBS and antibiotics were purchased from Gibco.

Cell Viability Assay/In Vitro Dark Cytotoxicity: In a typical cell viability experiment, ≈2000 cells per well were seeded in a 96-well plate in 200 µL of their respective culture medium. 24 h after cell growth, the cells were then treated with different concentrations of **APO_x-$ZnPc_y$** ($0 < [APO_x\text{-}ZnPc_y] < 100$ µg mL^{-1}) and, after 3 days, a colorimetric MTT assay of living cells was performed as follows. Cells were incubated with 0.5 mg mL^{-1} of 3-(4,5-dimethylthyazol-2-yl)−2,5-diphenyltetrazoliumbromide (MTT). Three hours after, MTT/medium solution was removed and the precipitated dark-purple crystals were dissolved in ethanol/DMSO (1:1, v/v) solution with gentle, round shaking for 20 min. The absorbance was read at 540 nm. The percentage of living cells was calculated based on a direct cor-

© 2024 The Author(s). Advanced Healthcare Materials published by Wiley-VCH GmbH

relation between the optical density (OD) and the number of living cells in the plate and was expressed as the ratio between the OD of treated cells and OD of control cells.

In Vitro Phototoxicity Assay: In vitro phototoxicity assays were performed with MDA-MB-231 cells seeded into 96-well plates at a concentration of $\approx 2 \times 10^3$ cells per well in 200 µL of culture medium and allowed to grow for 24 h. The cells were then incubated for 24 h in the presence or absence of the photosensitizer employed for the particular experiment ([**APO$_x$-ZnPc$_y$**] = 100 µg mL^{-1}). After incubation, cells were submitted, or not, to light excitation ($\lambda^{exc}{}_{max}$ = 630 nm, 1.45 J cm^{-2} or $\lambda^{exc}{}_{max}$ = 730 nm, 1.45 J cm^{-2}) for 10 min, using Cy5 and Cy7 light cubes, respectively) of EVOS5000 (ThermoFisher) microscope. Then, 48 h after irradiation, cell death was quantified by MTT assay as in the above-mentioned conditions.

Reactive Oxygen Species (ROS) Production: The day after being seeded in a 96-well plate in 200 µL of their respective culture medium, MDA-MB-231 cells were incubated with 100 µg mL^{-1} of **APO$_x$-ZnPc$_{60}$** for 24 h and submitted, or not, to light excitation ($\lambda^{exc}{}_{max}$ = 650 nm, 10 min, 1.45 J cm^{-2}). However, 45 min before excitation, cells were incubated with 20×10^{-6} M of 2′,7′-dichlorofluorescin diacetate (DCFDA / H_2DCFDA – Cellular ROS Assay Kit-ab113851). After excitation, cells were rinsed with culture media and fluorescence emission of 2′,7′-dichlorofluorescein (DCF) (λ^{exc} = 480 nm) was collected using the camera of standard fluorescence microscope.

In Vitro APO$_x$-ZnPc$_{60}$ Fluorescence Imaging: The day prior to the experiment, MDA-MB-231 cells were seeded onto bottom glass dishes (World Precision Instrument, Stevenage, UK) at a density of ≈100 cells cm^{-2}. Adherent cells were then washed once and incubated in 1 mL cell medium with or without **APO$_x$-ZnPc$_{60}$** at a concentration of 100 µg mL^{-1} for 24 h. Before visualization, cells were gently rinsed with cell media. Cells were then scanned via fluorescence microscopy excitating with Cy5 light cube of EVOS5000 microscope

Danio Rerio Embryos Handling for in Zebrafish Experiments: Wild-type AB zebrafish strain was purchased from Zebrafish International Resource Center (ZIRC) as embryos and were raised to adulthood in circulating aquarium system inside environmentally controlled room (28 °C, 80% humidity, 14 h light/10 h dark cycle), in the lab's facilities of Molecular mechanisms in neurodegenerative dementia (MMDN), Inserm U1198, Montpellier University, Montpellier. Only fish directly from ZIRC or their F1 offspring were used as egg producers to avoid inbreeding effects. Embryos were obtained from pairs of adult fish by natural spawning and raised at 28.5 °C in tank water. At 7 h post fertilization (hpf), embryos were examined under the microscope, and only embryos that developed normally and reached gastrula stage were selected for the study

Injection, Irradiation, and Imaging of MDA-MB-231 in Zebrafish Embryos: The MDA-MB-231 cells expressing Luc RFP were seeded in two 25 cm^2 flasks and incubated for 24 h. In one of the two flasks, the cells were treated with 100 µg mL^{-1} of **APO$_x$-ZnPc$_{60}$** solution. After 24 h incubation, the cells were trypsinized, centrifuged, and then resuspended in a sufficient volume of Phosphate-Buffered Saline (PBS) containing 2% Fetal Bovine Serum to have a cell concentration of 2×10^7 cells mL^{-1}. The two cell populations, with and without **APO$_x$-ZnPc$_{60}$**, were kept on ice until injection. The embryos at 24 hpf were divided into three groups: control group (without any injection), treatment with MDA-MB-231 Luc RFP cells alone, and treatment with MDA-MB-231 Luc RFP cells loaded with **APO$_x$-ZnPc$_{60}$**. The embryos were then anesthetized with tricaine solution at 17 mg mL^{-1} for 10 min prior to injection. Each embryo was placed in an agar mold for the microinjection of MDA-MB-231 cells expressing Luc RFP. Needles made of borosilicate glass with an internal diameter of 0.78 mm were loaded with 4 µL of the desired cell suspension. The cells were then injected into the embryos' yolk. Each embryo received 2–4 pulses of 10 nL cell suspension of 2×10^7 cells mL^{-1} to get 200–400 injected cells per embryo. The embryos were then placed in a 12 well plate (1 embryo per well in 400 µL of water), incubated at 30 °C and observed regularly after injection. One day later, the embryos were imaged and then submitted (or not) to light irradiation using RFP light cube of EVOS 5000 microscope. The wells were irradiated by 1 session of 10 min. of duration each. After 24 h, the effect of irradiation on the injected MDA-MB-231 cells was assessed by imaging the embryos with the same microscope. Final image analysis and visualization were performed using ImageJ-win32 software to adjust brightness and to remove out-of-focus background fluorescence.

Zebrafish Fluorescence Imaging: Zebrafish larvae of 24 hpf were manually dechorionated and then let develop for further 42 h in the above-mentioned conditions. The 72 hpf embryos were then anesthetized with tricaine solution at 17 mg mL^{-1} for 10 min prior to injection. The **APO$_x$-ZnPc$_{60}$** solutions at the concentration of 4.35 mg mL^{-1}, previously added of 10% penicillin–streptomycin, were directly injected via intra-venous injections. Each embryo received a total injected volume of ≈10 nL nanoparticle solution. Four hours later, the embryos were imaged using the Cy5 light cube of EVOS5000 microscope.

Statistical Analysis: Significance was carried out using Student t-test to compare the pared groups of data ("irradiated" vs "nonirradiated"). A p-value < 0.05 was considered statistically significant.

Supporting Information

Supporting Information is available from the Wiley Online Library or from the author.

Acknowledgements

The authors gratefully acknowledge Grant PID2021-123438NB-I00 funded by MCIN/AEI/10.13039/501100011033 and "ERDF A way of making Europe," Grant TED2021-130107A-I00 funded by MCIN/AEI/10.13039/501100011033 and Unión Europea "NextGenerationEU/PRTR", and Grant IT-1566-22 from Eusko Jaurlaritza (Basque Government). E.V.-S. acknowledges financial support from RyC program (RYC2022-037590-I).

Conflict of Interest

The authors declare no conflict of interest.

Data Availability Statement

The data that support the findings of this study are available from the corresponding author upon reasonable request.

Keywords

anthracene, imaging, photodynamic therapy, phthalocyanins, single-chain nanoparticles, zebrafish embryos

Received: May 7, 2024
Revised: June 18, 2024
Published online: July 7, 2024

[1] H. Sung, J. Ferlay, R. L. Siegel, M. Laversanne, I. Soerjomataram, A. Jemal, F. Bray, *CA: Cancer J. Clin.* **2021**, *71*, 209.
[2] A. J. Kerr, D. Dodwell, P. McGale, F. Holt, F. Duane, G. Mannu, S. C. Darby, C. W. Taylor, *Cancer Treat. Rev.* **2022**, *105*, 102375.
[3] A. Chow, K. Perica, C. A. Klebanoff, J. D. Wolchok, *Nat. Rev. Clin. Oncol.* **2022**, *19*, 775.
[4] A. Farzin, S. A. Etesami, J. Quint, A. Memic, A. Tamayol, *Adv. Healthcare Mater.* **2020**, *9*, 1901058.
[5] J. Shi, P. W. Kantoff, R. Wooster, O. C. Farokhzad, *Nat. Rev. Cancer* **2017**, *17*, 20.

© 2024 The Author(s). Advanced Healthcare Materials published by Wiley-VCH GmbH

21922659, 2024, 28, Downloaded from https://advanced.onlinelibrary.wiley.com/doi/10.1002/adhm.202401683 by Acibadem Mehmet Ali Aydinlar Universitesi, Wiley Online Library on [19/03/2026]. See the Terms and Conditions (https://onlinelibrary.wiley.com/terms-and-conditions) on Wiley Online Library for rules of use; OA articles are governed by the applicable Creative Commons License

[6] Y. Barenholz, *J. Controlled Release* **2012**, *160*, 117.
[7] Q. Chen, C. Liang, C. Wang, Z. Liu, *Adv. Mater.* **2015**, *27*, 903.
[8] N. Wang, X. Cheng, N. Li, H. Wang, H. Chen, *Adv. Healthcare Mater.* **2019**, *8*, 1801002.
[9] T. Zhang, Y. Li, J. Guo, W. Sun, Y. Lv, *Adv. Healthcare Mater.* **2024**, *13*, 2303615.
[10] S. Han, P. Xin, Q. Guo, Z. Cao, H. Huang, J. Wu, *Adv. Healthcare Mater.* **2023**, *12*, 2300311.
[11] B. Layek, S. Mandal, *Carbohydr. Polym.* **2020**, *230*, 115617.
[12] F. R. Wurm, C. K. Weiss, *Front. Chem.* **2014**, *2*, 49.
[13] G. Gunaydin, M. E. Gedik, S. Ayan, *Front. Chem.* **2021**, *9*, 686303.
[14] W. Jiang, M. Liang, Q. Lei, G. Li, S. Wu, *Cancers* **2023**, *15*, 585.
[15] J. M. Dąbrowski, in *Advances in Inorganic Chemistry*, *70*, (Eds: R. van Eldik, C. D. Hubbard), Academic Press, Burlington **2017**, 343–394.
[16] M. Gary-Bobo, O. Hocine, D. Brevet, M. Maynadier, L. Raehm, S. Richeter, V. Charasson, B. Loock, A. Morère, P. Maillard, M. Garcia, J.-O. Durand, *Int. J. Pharm.* **2012**, *423*, 509.
[17] X. T. Yu, S. Y. Sui, Y. X. He, C. H. Yu, Q. Peng, *Biomater. Adv.* **2022**, *135*, 212725.
[18] L. Chen, J. Huang, X. Li, M. Huang, S. Zeng, J. Zheng, S. Peng, S. Li, *Front. Bioeng. Biotechnol.* **2022**, *10*, 920162.
[19] D. Dinakaran, B. C. Wilson, *Front Bioeng Biotechnol* **2023**, *11*, 1250804.
[20] N. Plekhova, O. Shevchenko, O. Korshunova, A. Stepanyugina, I. Tananaev, V. Apanasevich, *Bioengineering* **2022**, *9*, 82.
[21] L. M. Moreira, F. V. dos Santos, J. P. Lyon, M. Maftoum-Costa, C. Pacheco-Soares, N. S. da Silva, *Aust. J. Chem.* **2008**, *61*, 741.
[22] L. B. Josefsen, R. W. Boyle, *Theranostics* **2012**, *2*, 916.
[23] P.-C. Lo, M. S. Rodríguez-Morgade, R. K. Pandey, D. K. P. Ng, T. Torres, F. Dumoulin, *Chem. Soc. Rev.* **2020**, *49*, 1041.
[24] N. Mehraban, P. R. Musich, H. S. Freeman, *Appl. Sci.* **2019**, *9*, 401.
[25] G. Ekineker, C. Nguyen, S. Bayır, S. Dominguez Gil, U. İşçi, M. Daurat, A. Godefroy, L. Raehm, C. Charnay, E. Oliviero, V. Ahsen, M. Gary-Bobo, J.-O. Durand, F. Dumoulin, *Chem. Commun.* **2019**, *55*, 11619.
[26] N. M. Hamelmann, J. M. J. Paulusse, *J. Controlled Release* **2023**, *356*, 26.
[27] *Single-Chain Polymer Nanoparticles: Synthesis, Characterization, Simulations and Applications*, (Ed. J. A. Pomposo), Wiley-VCH, Weinheim **2017**.
[28] M. Huo, N. Wang, T. Fang, M. Sun, Y. Wei, J. Yuan, *Polymer* **2015**, *66*, A11.
[29] R. Zeng, L. Chen, Q. Yan, *Angew. Chem. Int. Ed.* **2020**, *59*, 18418.
[30] J. P. Cole, J. J. Lessard, K. J. Rodriguez, A. M. Hanlon, E. K. Reville, J. P. Mancinelli, E. B. Berda, *Polym. Chem.* **2017**, *8*, 5829.
[31] D. Arena, E. Verde-Sesto, I. Rivilla, J. A. Pomposo, *J. Am. Chem. Soc.* **2024**, *146*, 14397.
[32] D. Arena, Ü. İşçi, M. Onofre, C. Nguyen, Z. Şahin, E. Verde-Sesto, A. Iturrospe, A. Arbe, M. Gary-Bobo, J. A. Pomposo, F. Dumoulin, *Mater. Adv.* **2024**.
[33] J. A. Pomposo, J. Colmenero, J. Kohlbrecher, A. Arbe, A. Sanchez-Sanchez, *Macromol. Rapid Commun.* **2015**, *36*, 1592.
[34] B. Robles-Hernandez, E. González, J. A. Pomposo, J. Colmenero, A. Alegría, *Soft Matter* **2020**, *16*, 9738.
[35] Y. Gao, H. Liu, S. Zhang, Q. Gu, Y. Shen, Y. Ge, B. Yang, *Phys. Chem. Chem. Phys.* **2018**, *20*, 12129.
[36] J. Zou, L. Li, J. Zhu, X. Li, Z. Yang, W. Huang, X. Chen, *Adv. Mater.* **2021**, *33*, 2103627.
[37] T. Mosmann, *J. Immunol. Methods* **1983**, *65*, 55.
[38] P. Mishra, B. Nayak, R. K. Dey, *Asia J. Pharm. Sci.* **2016**, *11*, 337.
[39] S. I. Dikalov, D. G. Harrison, *Antioxid. Redox Signal* **2014**, *20*, 372.
[40] R. White, K. Rose, L. Zon, *Nat. Rev. Cancer* **2013**, *13*, 624.

© 2024 The Author(s). Advanced Healthcare Materials published by Wiley-VCH GmbH

21922659, 2024, 28, Downloaded from https://advanced.onlinelibrary.wiley.com/doi/10.1002/adhm.202401683 by Acibadem Mehmet Ali Aydinlar Universitesi, Wiley Online Library on [19/03/2026]. See the Terms and Conditions (https://onlinelibrary.wiley.com/terms-and-conditions) on Wiley Online Library for rules of use; OA articles are governed by the applicable Creative Commons License